Glacier Recession on Heard Island, Southern Indian Ocean

Authors: Thost, Douglas E., and Truffer, Martin

Source: Arctic, Antarctic, and Alpine Research, 40(1) : 199-214

Published By: Institute of Arctic and Alpine Research (INSTAAR), University of Colorado

URL: https://doi.org/10.1657/1523-0430(06-084)[THOST]2.0.CO;2

Arctic, Antarctic, and Alpine Research, Vol. 40, No. 1, 2008, pp. 199–214

Glacier Recession on Heard Island, Southern Indian Ocean

Douglas E. Thost and Martin Truffer†*

*Corresponding author: The Australian Antarctic Division and the Antarctic Climate and Ecosystems CRC, Private Bag 80, Hobart, Tasmania 7001, Australia.
doug.thost@aad.gov.au
†Geophysical Institute, University of Alaska Fairbanks, 903 Koyukuk Drive, Fairbanks, Alaska 99775-7320, U.S.A.
truffer@gi.alaska.edu

Abstract

Glacier retreat has been widespread on Heard Island, an isolated 2745-m-high volcano in the southern Indian Ocean, since the first observations in 1947. This study represents the first quantification of the mass loss of a Heard Island glacier. Brown Glacier is 4.8 km long and is land terminating. A digital elevation model for the glacier was developed using a combination of static and kinematic differentially corrected GPS surveys and hand-held GPS elevations, and together with ground penetrating radar, was used to estimate the glacier's catchment area boundary. The 1947 extent of the glacier was estimated from an aerial photograph. The total ice covered area has decreased from an estimated 6.18×10^6 m^2 in 1947 to 4.38×10^6 m^2 in 2004. This corresponds to a loss of ~29% of the original area. During the same period the ice volume decreased by an estimated 1.743×10^8 m^3 ($\sim 3.06 \times 10^6$ m^3 a^{-1}), equating to an average thickness change of -0.50 m a^{-1}. The mass loss is consistent with limited temperature observations in the area that indicate a +0.9 °C warming over the same time span. Meteorological observations combined with an energy balance model demonstrate the impact of foehn winds on the mass balance of the upper slopes of the glacier. Between December 2000 and December 2003, repeat differentially corrected GPS surface surveys revealed an average surface change of -9.9 m in the ablation area and -5.9 m in the accumulation area, translating to an ice loss of $\sim 8.0 \times 10^6$ m^3 a^{-1}, or more than double the 57 year average rate. There is no indication of an increase in geothermal heat flux that could explain an ice loss of this magnitude. The increase in the rate of ice loss suggests the glacier is reacting to ongoing changes in climatic conditions rather than approaching steady state.

DOI: 10.1657/1523-0430(06-084)[THOST]2.0.CO;2

Introduction

The study of a glacier's response to climate change relies upon a detailed knowledge of the physical characteristics of the glacier (e.g. area, thickness, velocity) as well as the contributions of the components of the surface energy balance to the mass balance. Studies undertaken on glaciers in remote locations suffer from poor topographic models, infrequent visits, generally short observation periods for mass balance studies, and a limited suite of meteorological observations from which to construct detailed energy/mass balance models.

In this paper we describe the results of a reconnaissance glaciological and meteorological study of Brown Glacier, located on the northeast coast of subantarctic Heard Island in the southern Indian Ocean. The field work was conducted over two summer seasons separated by three years, defining the physical limits of the glacier and collecting meteorological and glacier velocity data. Here, we present the results of our field observations and the first quantitative measurements of the change in ice volume for a Heard Island glacier for the period 1947–2003, and compare it to recent changes in the period December 2000–December 2003.

Heard Island has been intermittently occupied since its discovery in 1833. There is no permanent settlement on the island, but a research station was maintained by the Australian Antarctic Division from 1947 to 1954 at Atlas Cove. Since then, the island has had only infrequent visits from the scientific and mountaineering communities. With the exception of the only other overwinter expeditions (1969–1970 and 1992–1993), all other visits were of short duration, generally during the austral summer. The most recent scientific expeditions took place in the austral spring–summer of 2000–2001, and 2003–04. Research stations have traditionally been established at Atlas Cove, and occasionally at Spit Bay (Fig. 1).

From 20 October to 29 November 2000 (hereafter, season one) a field camp was established near the base of Brown Glacier (BGC, Fig. 1). This site was reoccupied over the period 18 December 2003 to 20 February 2004 (season two).

Location and Site Description

Heard Island is an ice-covered, active composite shield volcano situated at 53°05′S, 73°30′E, approximately 4350 km southwest of Western Australia, 4850 km southeast of southern Africa, and 1650 km north of the Antarctic continent (Fig. 1). Together with the nearby McDonald Islands (45 km to the west), and Îles Kerguelen (433 km to the northwest), Heard Island is an emergent part of the extensive, predominantly igneous, submarine Kerguelen Plateau.

The island extends 43 km from Laurens Peninsula in the northwest to the end of Elephant Spit in the east. The bulk of the island is approximately circular in plan with a 20 km diameter, and consists of the Big Ben volcano with its active conical vent (Mawson Peak, 2745 m above sea level (a.s.l.); last seen active in the 2003–2004 summer) located on the southwestern edge of a broad summit plateau at ~2200 m a.s.l. The geologically

1523-0430/08 $7.00

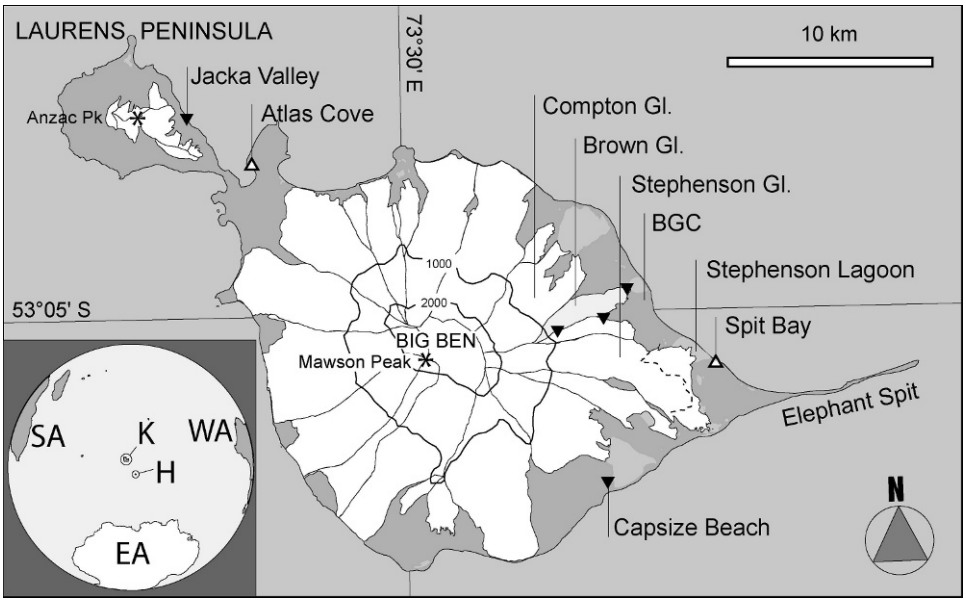

FIGURE 1. Map of Heard Island, showing the location of features discussed in the text. BGC: Brown Glacier campsite. Inverted black triangles indicate the location of local weather observation sites and automatic weather stations established during our field seasons, and open upright triangles are the location of long-term automatic weather stations recording air temperature and atmospheric pressure. The 1000 m and 2000 m contours are shown, as are the ice divides between individual glaciers (Ruddell, 2006). White areas are glacierized (at 1988–1991). The dashed line on Stephenson Glacier shows the approximate position of the ice front as of January 2006. Inset shows the location of Heard Island (H) relative to Îles Kerguelen (K), southern Africa (SA), western Australia (WA), and East Antarctica (EA).

younger Laurens Peninsula (Quilty and Wheller, 2000) is another distinct volcano, with Anzac Peak (715 m a.s.l.) at its summit, and is currently inactive.

Heard Island is spectacularly glacierized as a result of both its location south of the Antarctic Polar Front, a discontinuity between cold Antarctic Surface Water and less cold Subantarctic Surface Water (e.g. Taljaard and van Loon, 1984), and its height. As such, it provides an important point for monitoring climate change in a vast expanse of ocean. Glaciers cover approximately 70% of the island (257 km^2 in 1988; Ruddell, 2006). The majority of the island's major glaciers radiate from the summit region of Big Ben, with individual glaciers separated by well-developed lava buttresses (Allison and Keage, 1986; Quilty and Wheller, 2000). Nineteen of the glaciers have a flowline length exceeding 7 km and originate above 2000 m a.s.l. Many of the glaciers with northerly to southwesterly aspects are tidewater glaciers, whereas those with southerly to northeasterly aspects are land terminating, or terminate in lagoons well inland from the ocean. Laurens Peninsula is also glaciated, albeit on a much smaller scale than Big Ben (Ruddell, 2006).

Brown Glacier is one of the smaller Heard Island glaciers and has a comparatively simple geometry (Fig. 2). It is accessible along its entire length, and is land terminating. In February 2004 the glacier was 4.8 km long. Its accumulation area extended to ~1200 m a.s.l. and the lowest point of the terminus was then at 80 m a.s.l. The glacier boundary is poorly defined above 600 m elevation on its northwestern side, where it borders the Compton Glacier and above 550 m elevation on its southeastern side where it borders the Stephenson Glacier. At an elevation of ~400 m the glacier narrows from ~840 to ~600 m in width. A melt stream, active late in season one and seen to flow at various rates throughout season two, leads from the margin of stagnant ice on the northern side of the glacier at ~380 m a.s.l., flowing northeast to a prominent waterfall that drops ~60 m to the base of the cliffs.

GLACIER CHANGES ON HEARD ISLAND

The limited observations that exist on Heard Island glacier fluctuations, mainly derived from aerial photography and more recently, satellite imagery, are summarized by Ruddell (2006). He reports widespread glacier recession that is more pronounced on the eastern side of the island, due to the greater sensitivity to climate change there; on the western side the glaciers originate from high up on the mountain and lose most of their mass through calving into the ocean, whereas their eastern counterparts have accumulation areas at lower altitudes and many of the glaciers are land terminating, making them likely to be more sensitive to climate variations (Ruddell and Allison, 1998; Ruddell, 2006).

Photographic and other records showed no apparent change in glacier extent between 1874 and 1929, but from 1947 to 1955 minor glacier recession was occurring (Budd, 2000). It was the 1963 expedition that obtained the first evidence of major recession in most of the island's glaciers (Budd, 1964, 1970, 2000; Budd and Stephenson, 1970). Budd (2000) divided periods of observation and glacier response into an initial phase of minimal change (1947–1955), a subsequent period of rapid change (1963–1971) in which a complex pattern of asynchronous glacier retreat and readvance was observed, followed by continuing glacier recession (post-1983). These fluctuations in glacier retreat and advance are correlated with changing air temperatures (and perhaps precipitation and cloud cover), and indicate sensitivity of the Heard Island glaciers to Southern Ocean climate change, as well as interactions between climate and glacier aspect, topography, and altitude range (Ruddell and Allison, 1998; Budd, 2000; Ruddell, 2006; Thost and Allison, 2006). Ruddell (2006) calculated a loss of 11% of ice-covered areas and used scaling relations to estimate an 11.25% decrease of ice volume from 1947 to 1988.

At present some of the Heard Island glaciers are undergoing a period of rapid change. For example, a comparison between that portion of a high-resolution *Quickbird* satellite image covering Stephenson Lagoon (taken on 17 January 2003) and a lagoon bathymetry survey track undertaken by us on 17 January 2004 (Thost et al., 2004) revealed that the front of Stephenson Glacier had retreated approximately 200 m in one year. In January 2004 Stephenson Lagoon became continuous to the south coast. A more recent *Quickbird* image (30 January 2006) indicates the

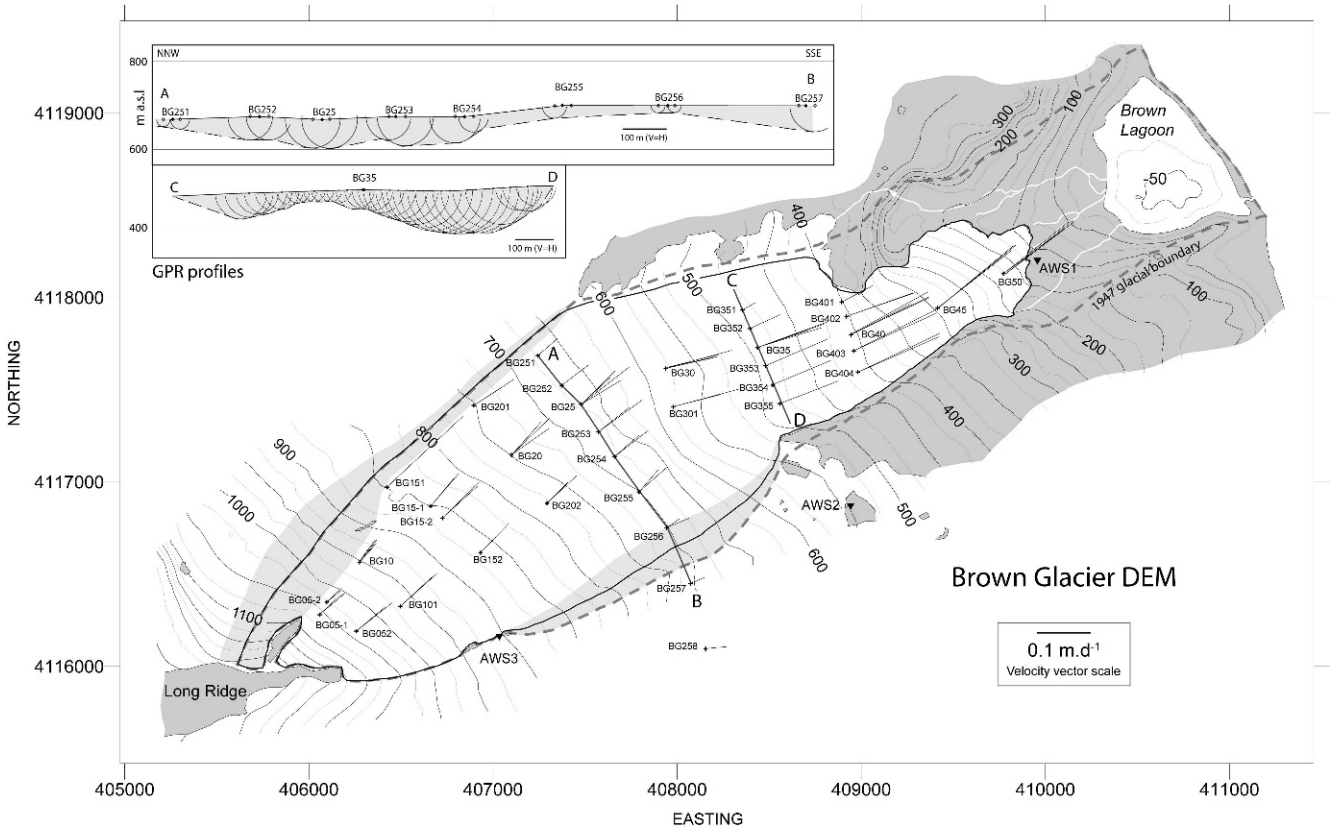

FIGURE 2. Digital Elevation Model (DEM) of Brown Glacier. The DEM incorporates lagoon bathymetry. Contour interval 25 m. Survey points (+) and velocity vectors for both field seasons are shown. The location of three AWSs are indicated by inverted triangles. The fine solid outline is the estimated boundary of the glacier at January 2004. Uncertainties in the glacier boundary above ~550 m are indicated by the shaded regions. The bold dashed outline is the estimated extent of the 1947 glacier. Major drainage channels from the upper glacier and the terminus are shown by the white lines. Rock outcrops are shown in dark gray. Insets show the results from ground penetrating radar (GPR) across the BG25 (A–B) and BG35 (C–D) survey lines. The DEM contains no elevation information for Long Ridge (lower left). Horizontal datum: WGS84. Projection: UTM Zone 43.

retreat of Stephenson Glacier to be continuing (terminus position shown as a dashed line on Fig. 1).

Photographs of Brown Glacier taken in December 1947 and December 2003 (Figs. 3a and 3b) demonstrate the changes that have taken place. The 1947 aerial photograph (Fig. 3a) shows the glacier to be near its maximum extent, reaching the ocean as an active tidewater glacier with terminal ice cliffs at least 25 m high, with the ice surface just below its lateral moraines. Each subsequent visit showed the glacier to be retreating (Fig. 4). By March 1963 the ice cliffs were gone, and Brown Glacier had retreated more than 100 m inland, leaving a small lagoon separated from the sea by a boulder beach (Budd and Stephenson, 1970, their Plate 5), and by 1971 had retreated a further 350 m from the coast (Budd, 2000), terminating in a proglacial lagoon. In 1987, the central portion of the terminus was close to the 1980 position but the lateral margins had each retreated by about 200 m. During this period the terminus narrowed and became grounded, and only a very small quantity of ice calved into the lagoon. By 2004, a further retreat of about 350 m had taken place (Figs. 3b and 4). Total retreat for the period 1947–2004 was 1.17 km.

Methods

SURVEY DESIGN

The most recent published map available for Heard Island is derived from a digital elevation model (DEM) created from *RadarSat* data (Ryan, 2004). The controls for this map were corner reflectors located along the coast, and the DEM is not well constrained at higher altitudes. We used this map prior to season one in our selection of potential survey sites on the glacier surface. The sites along the glacier's length were named BG05, approximately 500 m from the head of the glacier, to BG50 at the terminus and are spaced at approximately 500-m intervals (Fig. 2). Two transverse networks of survey sites were established during season one, at the elevation of BG35 and BG40. In season two a higher and more extensive transverse survey was established at the elevation of BG25, to better define the glacier where it shares common boundaries with the Compton and Stephenson glaciers. In season two, sites above BG35 had an additional survey site added at approximately the same elevation, offset by 200–300 m. Each survey site was marked using a bamboo pole (season one) or a 2.4-m-long white fiberglass pole (season two).

STATIC AND KINEMATIC DIFFERENTIAL GPS SURVEYS

A GPS base station was set up near our camp during season one and reoccupied during season two (Fig. 4). A total of three static differentially corrected GPS (DGPS) surveys were made at each site on the glacier, defining two epochs for each season. Average surface ice velocity at each survey site was determined for each epoch by measuring the difference in position of the survey marker divided by the number of days between surveys. The errors in vertical position are estimated at 0.02 m for these short baseline

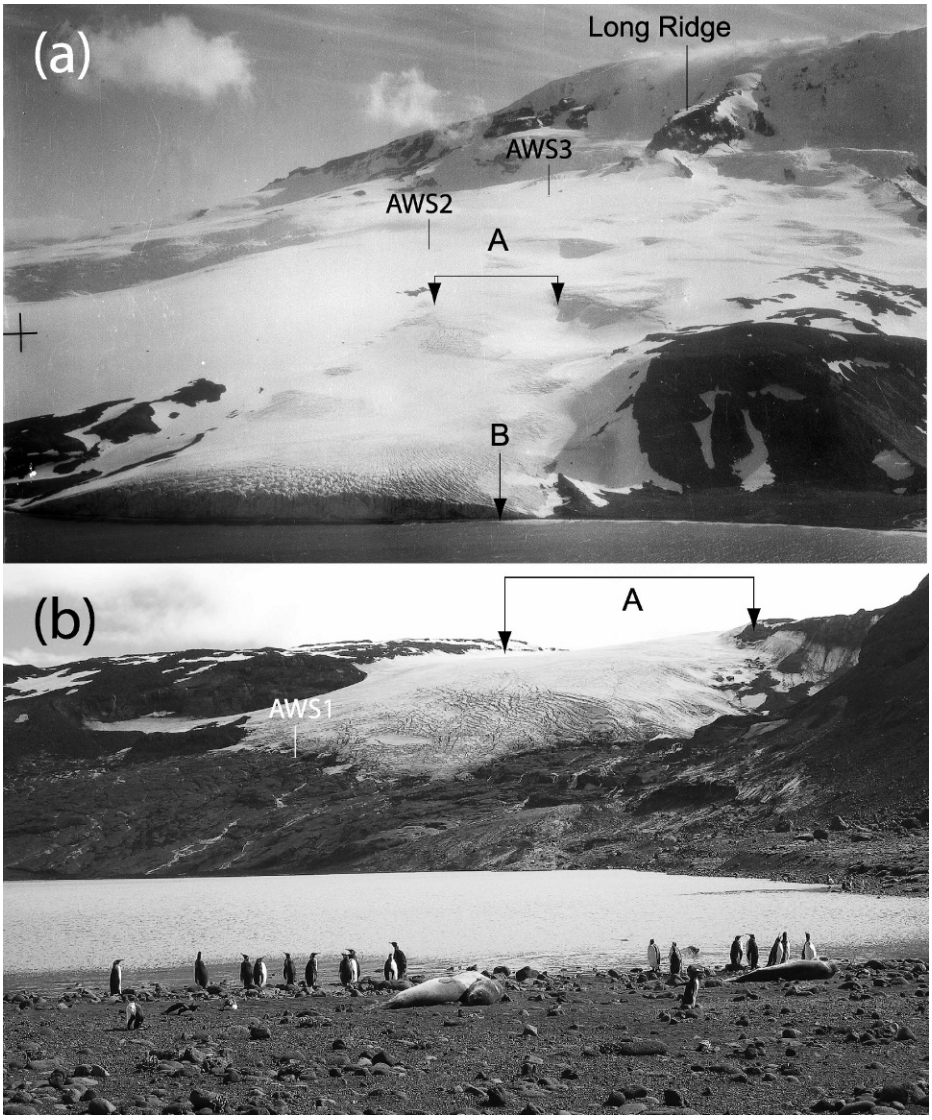

FIGURE 3. Photographs of Brown Glacier. (a) Aerial photograph taken on 13 December 1947, showing Brown Glacier as a tidewater glacier with a ca. 25-m-high terminal ice cliff. Feature "A" bracketed by arrows is also shown in (b), and marks the width of the glacier at that elevation ca. year 2000. Feature "B" is the approximate vantage point from which the photograph in (b) is taken. Also shown are the locations of Long Ridge, which bifurcates and defines the upper catchment of the glacier at ca. 1200 m a.s.l., and the location of AWS3, and approximate location of AWS2, in 2003–2004. Photo by R. Swan, Royal Australian Air Force photo 620, © Commonwealth of Australia, Australian Antarctic Division. (b) Brown Lagoon and Brown Glacier, as they appeared on 30 December 2003 from the gravel bar separating the lagoon from the ocean. Feature "A" is also shown in (a). The location of AWS1 is indicated.

(<5 km) surveys. This results in a ± 0.003 m d^{-1} velocity error for the shortest epoch.

Kinematic DGPS surveys were made along longitudinal and transverse routes on the glacier surface (Fig. 5), as well as the lateral moraine ridges, the glacier terminus position, rocky outcrops along the glacier margin, and the lagoon shoreline. These data were recorded at five second intervals and post-processed using *Leica Ski-Pro* software. The GPS antenna was fixed to the surveyor's backpack. We estimate the uncertainty in vertical position as ± 0.15 m.

VOLUME CHANGE BETWEEN SEASON ONE AND TWO

The first DGPS kinematic surveys on the glacier surface in season one (20–23 November 2000) were repeated in season two (lower glacier, 2 January 2004; upper and middle glacier, 1–2 February 2004). It was not possible to exactly retrace our season one survey due to increased crevassing during season two. The season two surveys were corrected in elevation to the beginning of the field season (late December 2003), by adding the total surface lowering measured at the nearest of 19 ablation markers on the day of the survey. In November 2000 most sites on the glacier were still accumulating snow. By mid-January 2001 melting of up to 1 m was noted at the lower sites (P. Scott, personal communication, 2001). In an attempt to remove seasonal effects we have assumed that the additional accumulation until late December roughly balances December ablation and that the survey comparison is from December 2000 to December 2003.

The corrected elevation difference at crossing points between the season one and two kinematic surveys was used to calculate the total volume change of the glacier from December 2000 to December 2003. The glacier was divided into a regular grid, and a thickness change was calculated for each point as a distance weighted average of all the crossing points within a 1000-m radius.

LOCAL DEM

We compared our DGPS results to the *RadarSat* map after first subtracting a 40-m geoid-ellipsoid correction from the DGPS data. Comparisons over land showed random differences averaging about 20 m. A more accurate local DEM was created using the season two field GPS data, combining DGPS data obtained during repeat survey measurements and static surveys of marker canes, and hand-held GPS data obtained during daily excursions on the glacier surface. Although less accurate than the DGPS points (particularly in elevation), direct comparison between the GPS and coincident DGPS elevations revealed consistent daily errors (<5m in position, and as much as 20 m in elevation), which

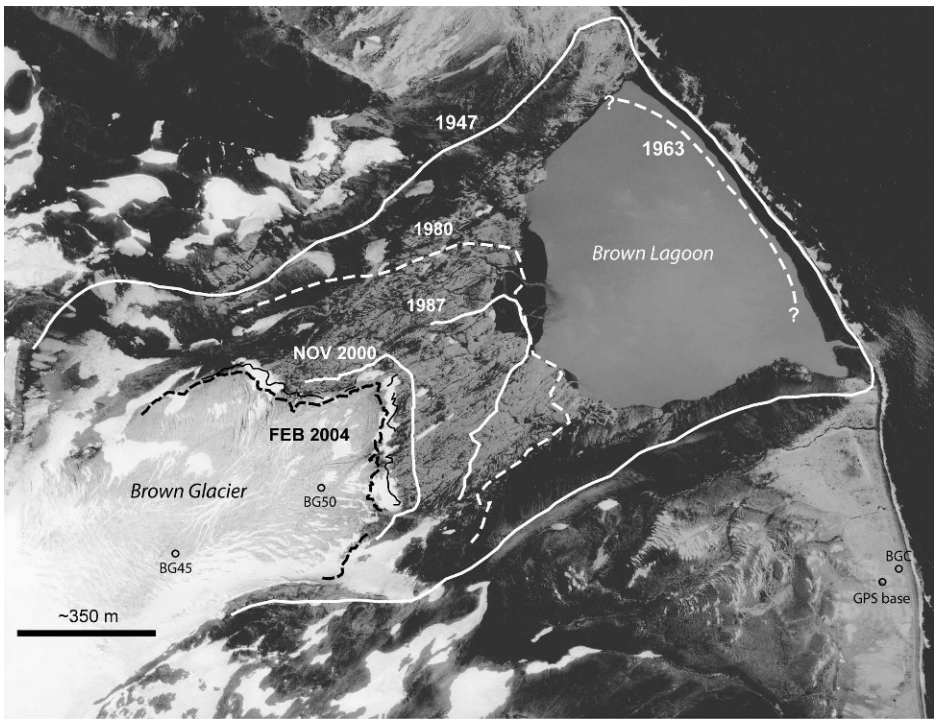

FIGURE 4. Terminus position of Brown Glacier at various times since 1947. The 1963 position is estimated from an oblique photograph taken from a nearby hill (Budd and Stephenson, 1970). The position of the 1980 (dashed) and 1987 terminus are plotted from aerial photographs. The 23 November 2000 and 17 February 2004 positions were surveyed using DGPS. The December 2003 survey is shown as a fine black line between the latter two, and is not labeled. Also shown are the location of the campsite (BGC) and the DGPS base station. The background image is from the *Quickbird* satellite, acquired on 12 January 2003 (image courtesy of the Australian Antarctic Division, © DigitalGlobe 2003, used with permission).

could be compensated for by the addition or subtraction of an average error on the day of observation. The GPS points provided extra surface elevation data where none existed previously, particularly on the rock outcrops bounding the lower glacier, but also on general transit routes from AWS2 to the highest survey points on the glacier. It was not possible to access all areas on the glacier and its surrounding rock outcrops, and we have estimated elevations at a number of locations (cliff lines, ice falls, crevassed areas). Estimates of height were made by extending known heights determined by (D)GPS with reference to local oblique photos, as well as the high-resolution *Quickbird* image. The DEM (Fig. 2) was created with a 50-m grid spacing using kriging in *Surfer* v8.0.

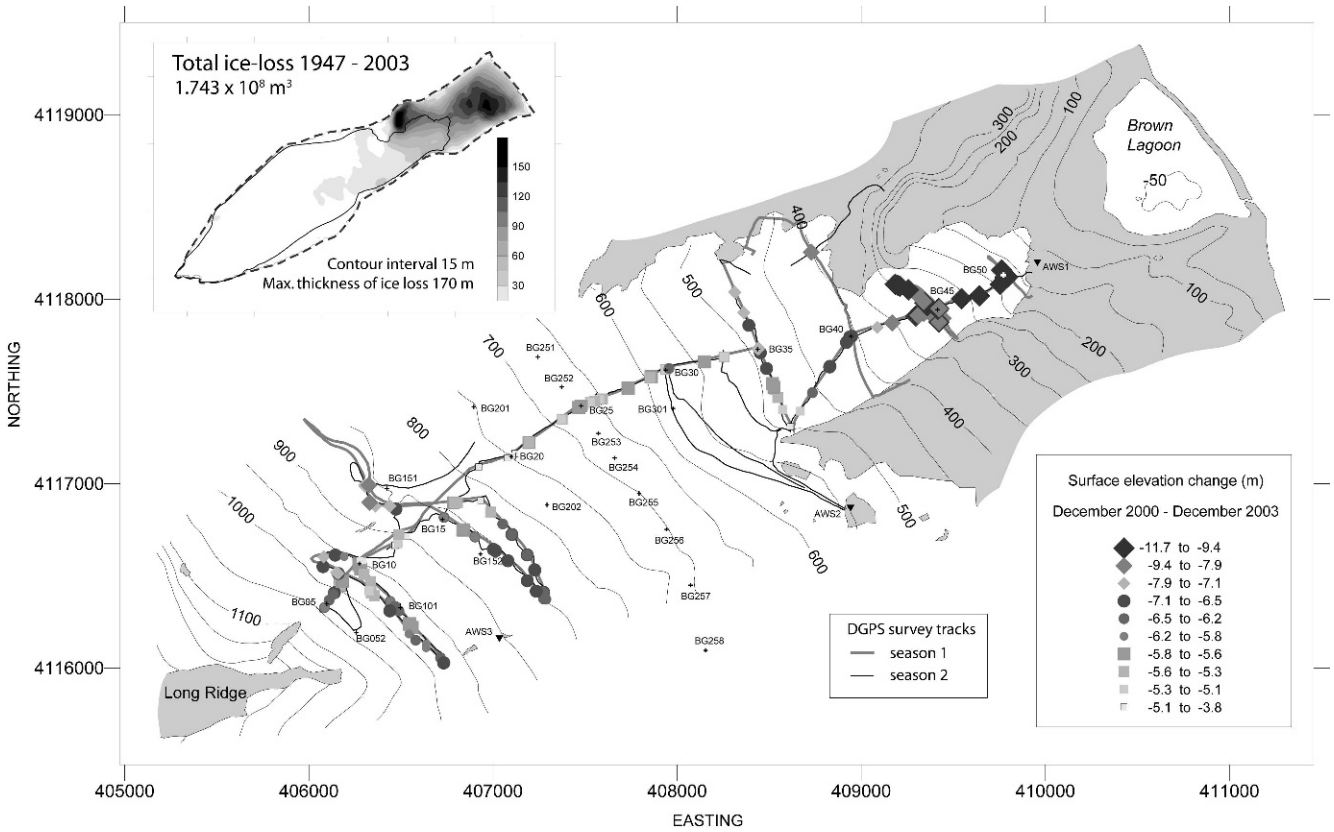

FIGURE 5. The change in surface elevation (m) between December 2000 and December 2003, as determined by repeat DGPS surveys. Major DGPS survey tracks are also shown. Inset shows the estimated total ice loss for the period 1947 to 2003.

TABLE 1

Meteorological stations deployed during season one and two. All shields and screens were naturally ventilated. AWS2 (installed season 1) operated for 22 months from October 2000. Height above ground level (a.g.l.) is given for various instruments. Air temperature (T), relative humidity (RH), wind speed (WS), wind direction (WD), solar radiation (SR). ^ Indicates only intermittent operation of RH sensor at AWS3. * Indicates only one month operation.

Station (season)	Height a.s.l. (m)	Meteorological variable	Instrumentation
Jacka Valley (2) and	~3	T and RH	Temperature Technology T-TEC 6-1C datalogger
Capsize Beach (2)	~40		in Stephenson screen, 1.0 m a.g.l.
AWS1 (2) and	115	T and RH^	Vaisala HMP45D in 9-plate radiation shield, 1.2 m a.g.l.
AWS3 (2)	920	WS and WD	Vaisala WMS302, 2.3 m a.g.l.
		SR	Kipp & Zonen CM3 pyranometer
BG35 (1) and	498	T	Aanderaa 3455 in 6-plate 60 mm radiation shield, 1.5 m a.g.l
AWS2 (2)	550	WS	Aanderaa 2740, 1.5 m a.g.l.
AWS2 (1)	550	T	FS23D thermistor in radiation shield, 2.0 m a.g.l.
		RH*	Vaisala HMP35D in radiation shield, 2.0 m a.g.l.
		WS*	Aanderaa 2740, 4.0 m a.g.l.
		SR	Middleton EQ08 pyranometer

BROWN GLACIER 1947

A 1947 glacier surface DEM of Brown Glacier was reconstructed by assuming a terminus ice front height of 20 m at the seaward shore of the lagoon, and interpolating slightly convex down-glacier contours (as is commonly the case in ablation zones) between the surveyed moraine crests. In the 1947 aerial photograph of Brown Glacier we note that two small outcrops at the lateral margin of the glacier between 900 and 950 m a.s.l. are visible (Fig. 3a). The lower of these outcrops was the site for AWS3 in season two, and the two outcrops looked similar in size in 2004. In our reconstruction of the 1947 ice surface we have therefore assumed that the area above 650 m has not changed significantly.

LAGOON BATHYMETRY

In addition to the land-based surveys, we used a small inflatable boat equipped with an acoustic depth sounder (transducer: 100 W (RMS), 200 KHz, 20° beam width), and a hand-held GPS to compile 211 soundings to produce a bathymetric map of Brown Lagoon. The accuracy of the soundings was checked against a weight lowered on a tape measure at several locations up to depths of 30 m, and found to be within 1 m. The soundings are considered to be accurate to ±5% at depths greater than 30 m.

ICE THICKNESS

Ice thickness was measured with a portable low frequency ground penetrating radar (GPR) unit (Narod and Clarke, 1994). Both 5- and 10-m dipole antennas were used, producing frequencies of about 8 and 4 MHz respectively, and the high frequencies gave good returns despite Brown Glacier being temperate. We used a value of 168 m μs^{-1} for the wave speed in ice, and estimate errors (associated with density variations between ice and firn, as well as reading the two-way travel time from the scope meter) to be ±10% of the reported thickness.

One detailed profile across BG35 (Fig. 2, profile C–D) and several spot depths along the glacier were recorded. Two less detailed profiles were acquired at the elevations of BG25 (Fig. 2, profile A–B) and BG20. Reflections are assumed to be within a plane perpendicular to the glacier surface, which is reasonable when the profiles are in a transverse direction in a simple valley-glacier geometry. Each measurement then defines a return semi-circle, and lines tangential to these circles define the glacier bed. All antenna survey positions were also surveyed with DGPS.

METEOROLOGICAL MEASUREMENTS

Over the course of our two field seasons, we deployed a number of automatic weather stations (AWSs) at different locations (Fig. 2). The units and their instrumentation are summarized in Table 1.

During season one our team erected a 4-m-high AWS (located at site AWS2) on the northwestern edge of a boulder-covered basaltic glacial pavement (~20,000 m^2) at 550 m a.s.l. Although many instruments failed on this AWS, the 2-m air temperature was recorded (on average) every two hours for 22 months. The extreme variability in temperature at this site, including very high temperatures for such an elevated position, prompted us to deploy another two AWSs during season two (AWS1 at the terminus of the glacier, 115 m a.s.l.; and AWS3 on a ~200 m^2 basaltic glacial pavement at 920 m a.s.l.), as well as a replacement for AWS2.

SURFACE ABLATION MEASUREMENTS

Campbell Scientific SR50 sonic ranger sensors (SRS) were installed at BG35 (season one and two) and BG50 (season two). These sensors recorded the distance to the snow/ice surface every 30 minutes, with an accuracy of 0.01 m. During season 2 the SRS at BG35 only operated reliably between 1 and 13 January. The height of the site survey markers above the snow/ice surface was routinely measured throughout season 2. Net ablation for January at each site was calculated by interpolating between measurements made either side of the beginning and end of the month. Errors associated with this interpolation are estimated at ±0.1 m for most sites, except for some sites on the BG25 profile which were added during January, with extrapolation back to the beginning of January estimated to be in error by ±0.2 m.

MELT CALCULATIONS

Surface melt rates at the major longitudinal survey sites were calculated for the month of January using a surface point energy balance model (EBM) (Brock and Arnold, 2000). The EBM requires two sets of inputs: first, hourly meteorological measure-

TABLE 2

Input parameters for the energy balance model. Aspect is given in degrees counterclockwise from south.

Station	Latitude (°E)	Longitude (°S)	Elevation (m)	Slope (°)	Aspect (°)	Albedo	z_0 (m)
BG50	53.079	73.653	179	18	127	0.25	0.0050
BG45	53.080	73.647	296	14	127	0.37	0.0036
BG40	53.082	73.640	407	10	115	0.48	0.0021
BG35	53.082	73.633	492	10	108	0.60	0.0007
BG30	53.083	73.625	582	10	102	0.80	0.0007
BG25	53.085	73.618	673	10	126	0.80	0.0007
BG20	53.087	73.613	749	11	133	0.80	0.0007
BG15	53.090	73.607	863	13.5	132	0.80	0.0007
BG10	53.092	73.600	952	13.5	139	0.80	0.0007
BG05	53.094	73.597	1027	18	131	0.80	0.0007

ments of incoming shortwave radiation, air temperature, vapor pressure, and wind speed; and second, the site factors of slope, aspect, latitude, longitude, albedo, elevation, aerodynamic roughness length (z_0), and, where the site is not co-located with the meteorological station, temperature lapse rate. For a detailed description of the model and its underlying assumptions, the reader is referred to Brock and Arnold (2000).

Meteorological data were recorded at AWS1, 2, and 3 during January 2004. Hourly average meteorological variables were calculated for each longitudinal site on the glacier assuming linear variation between each of the meteorological stations (i.e. the lapse rate between AWS1 and 2 was used to calculate the air temperature at sites BG50 to BG30, and the lapse rate between AWS2 and 3 was used to calculate the temperature at sites BG25 to BG05). Data gaps were filled using parameterizations based on coincident data. In particular, vapor pressure had to be estimated for 77% of January at AWS3 due to the intermittent operation of the RH sensor there, using results from AWS1. Estimates for surface albedo and z_0 were made based on our perception of average surface conditions, with reference to Paterson (1994, p. 59 and 63). EBM input parameters are presented in Table 2.

Climate of Heard Island

The climate of Heard Island has been described as a contrast between large-scale regional uniformity (due to its location in the zone of strong westerly winds near the oceanic Antarctic Polar Front) and small-scale regional variability (due to its mountainous nature; Thost and Allison, 2006). The oceanic setting leads to a low seasonal range in temperature, persistent and generally low cloud cover, frequent precipitation, and strong winds. Wind flow over the 2745-m-high island is highly disturbed (e.g. Beggs et al., 2004) and causes significant variability in the patterns of both precipitation and snow accumulation, localization of violent wind gusts and foehn winds, and the formation of a range of orographic cloud types over and downwind of Big Ben. There are also strong gradients in temperature, wind speed, and precipitation with elevation.

Existing meteorological records from Heard Island are sparse and of short duration, with the longest records being restricted to two accessible coastal localities at Atlas Cove and Spit Bay (Fig. 1). There is little quantitative information on the regional variability or microclimate. The following description of the climate of Heard Island is summarized from Thost and Allison (2006).

The most complete record of air temperature is from Atlas Cove at the western extreme of the Big Ben massif, and runs from February 1948 until January 1955, with additional observation from AWSs in 1982–1983, and April 1997–present. The most noticeable feature of the temperature regime at Atlas Cove is the typical maritime low range in the seasonal variability: monthly averages range from 0.3 to 4.1 °C (Fig. 6a).

Fewer observations are available from Spit Bay, with temperature records spanning the period April 1997 to present. For the period 1997–2005, Spit Bay experienced consistently higher average monthly temperatures than Atlas Cove from December to April inclusive (Fig. 6a). The average monthly difference between the two sites was as much as 1.3 °C in December 1998. The difference between Spit Bay and Atlas Cove is even more obvious when extreme monthly maximum temperatures are compared (Fig. 6b). These temperature extremes are a result of dynamic modification of the predominantly westerly airflow by Big Ben, resulting in frequent and sometimes intense foehn winds along the northeast and east coasts (see below).

The only other site on Heard Island for which there is a full seasonal temperature record is at AWS2 adjacent to Brown Glacier (Fig. 2). The 2 m air temperature record covers the period November 2000 to August 2002. Because of the elevation of the site, the average monthly temperatures are some 3 to 4 °C below temperatures recorded at Atlas Cove and Spit Bay (Fig. 6a), and an extreme minimum of −12.3 °C (June 2001) was recorded over the 22 months of data.

AWS2 was subject to more frequent and stronger high temperature events than Spit Bay, and these influence the maximum temperatures and the temperature variability at the site. Despite the elevation, it can be much warmer at AWS2 than at the coast. This is apparent from comparison of extreme maximum temperatures at AWS2 and Atlas Cove (Fig. 6b), with AWS2 recording extreme monthly maxima during its period of operation that exceed any maxima at Atlas Cove for either the 1948–1955 or 1997–2005 epochs. An extreme maximum of 19 °C was recorded at AWS2 in March 2001. The standard deviation of temperature records at AWS2 (Fig. 6c) is even greater than at Spit Bay.

Mean annual precipitation at Atlas Cove for the 1948–1954 epoch was 1381 mm (1σ = 163 mm), with some form of precipitation occurring on 75% of days during the period. At Spit Bay, precipitation was recorded between March 1992 and February 1993. The total rainfall over this period was 1971 mm; nearly 300 mm more than for any year recorded at Atlas Cove from 1949 through 1954. The only other additional records suggest precipitation is highly variable around the island: synchronous observations of precipitation in January 2004 recorded totals of 298.9 mm from Jacka Valley, 189.9 mm from Spit Bay, 221.5 mm from Capsize Beach, and 482.9 mm from the Brown Glacier camp. In comparison, the average January precipitation for Atlas Cove (1948–1954) was 139.3 mm.

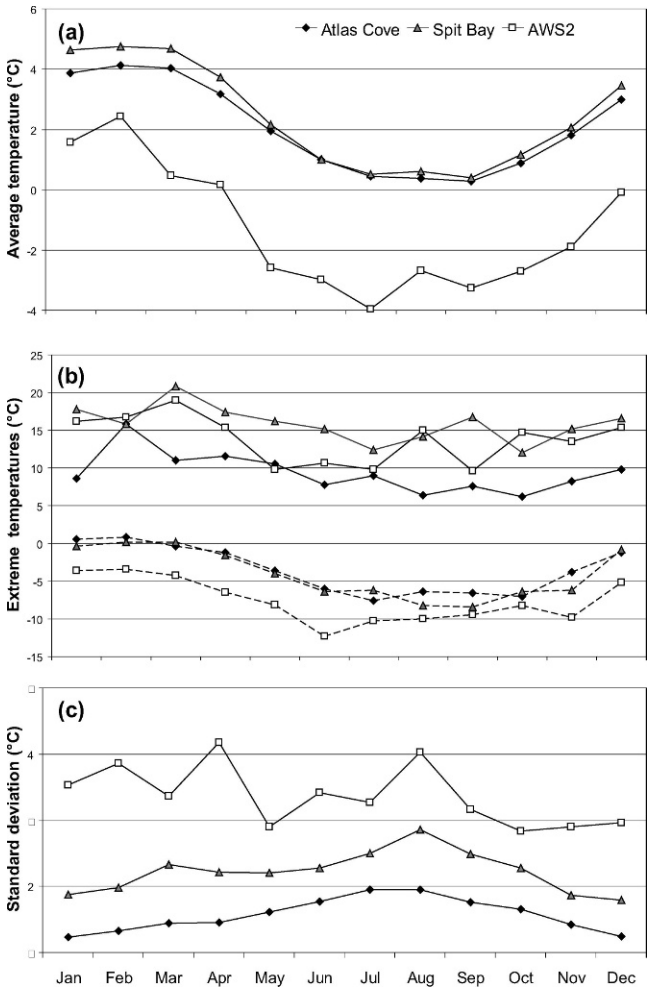

FIGURE 6. Monthly surface air temperature data (°C) for three Heard Island sites with data between 1998 and 2005. Atlas Cove (3 m a.s.l., site no. 300005, WMO no. 95997) and Spit Bay (12 m a.s.l., site no. 300028, WMO no. 94997) data are from modified oceanographic buoys for the period January 1998 to December 2005. Data from AWS2 (adjacent to Brown Glacier, 550 m a.s.l.) are for November 2000 to August 2002. (a) Mean monthly temperature; (b) extreme maximum (solid lines) and minimum temperatures (dashed lines); (c) standard deviation.

Average monthly wind speed at Atlas Cove ranges from a low during December–January of 7.2 m s^{-1} to a high during August–September of 9.3 m s^{-1}. At Atlas Cove, 20% of winds were from southwest and 77% from directions within the sector SSW–NW.

Elsewhere on the island, records of wind speed and direction cover a much shorter period, and observations are affected by local topography (e.g. Beggs et al., 2004). Wind speed increases markedly with elevation: the monthly mean wind speed for January 2004 recorded at AWS1 was 4.5 m s^{-1} compared with 10.6 m s^{-1} for AWS3 (Table 3). Gust speeds are intensified by steep lee slope topography (e.g. Lilly and Zipser, 1972; Brinkman, 1974; Miller and Durran, 1991), and squalls exceeding 50 m s^{-1} are not a rare phenomenon on the slopes of Big Ben: maximum daily gusts exceeded 50 m s^{-1} at AWS3 on 13 days between 25 December 2003 and 25 January 2004.

FOEHN WINDS

Anecdotal reports of wind storms and rapid thaws are common from climbing expeditions to the island (e.g. Chester, 1983); however, data associated with these events are rare. Shaw (1955) noted only one instance at Atlas Cove when predominantly easterly winds resulted in 3–5 °C higher temperatures, and 10–20% lower relative humidity, attributed by him to a slight foehn effect. In contrast, the 1992 over-wintering expedition at Spit Bay recorded a maximum temperature of 21.6 °C in April, and on nine days spread across four months (April, June, September, February) recorded higher temperatures than the maximum of 14.4 °C recorded at Atlas Cove in the period 1947–1955 (Green, 1993). Due to the predominantly southwest to northwesterly winds, Atlas Cove is rarely in the lee of Big Ben and is less likely to experience foehn winds (Green, 1993), whereas the opposite is true at Spit Bay.

In the period April 1997 to April 2005, Spit Bay AWS recorded 137 days when the air temperature exceeded 10 °C compared with only 10 days at Atlas Cove (Australian Bureau of Meteorology, unpublished data). In the absence of wind speed data, and acknowledging that Spit Bay often receives more direct solar radiation than Atlas Cove, it is possible that many of these high temperature events may be in error by up to several degrees, as a result of radiative heating of the naturally ventilated sensor shield (e.g. Arck and Scherer, 2001).

Our initial observations during season one indicated that these events were more likely to be the results of a meteorological phenomenon than poorly ventilated temperature sensors. On 25 November 2000 the AWS at BG35 recorded a temperature rise from 1.2 to 10.8 °C between 08:30 and 09:00 local time (UTC + 5), coincident with rising wind speed from 3.6 to 8.0 m s^{-1} between 08:30 and 10:00 (half hour averages), gusting to 29.5 m s^{-1}. The SRS recorded a reduction of 0.13 m in snow surface height in 4.5 hours, prior to the unit being turned off. AWS2 recorded a peak hourly average temperature of 13.5 °C for this event, with a RH of 28%. Temperatures at AWS2 fell below 0 °C early that evening. Early in the morning of 26 November the wind speed and temperature increased again and later that day the waterfall at the northern edge of the Brown Glacier valley was observed flowing for the first time that season, suggesting significant melting was occurring. Temperatures at AWS2 were above 5 °C for another ~20 hours, and hourly wind speed averages of 21 m s^{-1} were recorded. Temperatures peaked at 12 °C with a RH of 16%.

During season two, the three AWS installed by us recorded similar events. Results of hourly mean temperature, RH, wind speed, and wind direction for January 2004 are presented in Figure 7 and summarized in Table 3. During January the hourly mean air temperature recorded at AWS3 exceeded that at AWS2 and AWS1 for 53 hours and 28 hours, respectively. Of interest are the differences in timing for peak temperatures and the pronounced oscillations in temperatures between the two upper stations, corresponding to similar oscillations in wind speed and direction. Not all the high temperature events (identified in Fig. 7 by periods when the air temperature at AWS3 exceeded 0 °C) can be classified as classic foehn winds (i.e. downslope); some warm wind storms between 1 and 9 January are associated with northwesterly winds. Other events seem more obviously foehn-like, with high temperatures, low RH, high wind speeds, and originating from the southwest to westerly sector (9–11, 17–20, 29 January).

The mechanism for the formation of foehn winds has been investigated by observational and numerical studies of flow past mountain ranges and isolated topography (e.g. Klemp and Lilly, 1975; Ólafsson and Bougeault, 1996; Schär and Durran, 1997; Bauer et al., 2000). The classic explanation for their generation is by the uplift and cooling of stable air accompanied by moisture loss as the air is forced over a mountain range, followed by

TABLE 3

Summary of meteorological data for January 2004 for the three automatic weather stations (AWSs) adjacent to Brown Glacier. Locations are shown in Figure 2.

Station (elevation, m a.s.l.):	AWS1 (115)			AWS2 (550)			AWS3 (920)		
Temperature (°C)									
avg. (*std dev*), max., min.	5.0 (*2.6*)	15.0	0.3	1.7 (*3.5*)	15.5	−3.4	0.5 (*4.4*)	12.9	−5.5
Relative Humidity (%)									
avg. (*std dev*), max., min.	77 (*14*)	100	26						
Windspeed (m s^{-1})									
avg., max. 10 minute, max. gust	4.5	10.4	32.5	10.1	33.1	52.3	10.6	36.8	62.5
Dominant directions (degrees true)									
1st, 2nd, 3rd	310	290	320				270	315	220

rewarming on descent in the lee of the range at the dry adiabatic lapse rate (e.g. Barry and Chorley, 1976, p. 143). However, there is not always accompanying upwind precipitation, and standing waves, amplified by a deep inversion layer, which force air from higher levels (with high potential temperatures) to intersect lee slope topography are another mechanism for their generation (Klemp and Lilly, 1975). Modeling by Durran (1986) suggested that the presence of an inversion is a prerequisite for a significant foehn windstorm.

Our observed oscillations in temperature, wind speed, and direction at different elevations may be the result of turbulent mixing between two primary waves produced as air flows both over and around Big Ben (see Schär and Durran, 1997): one a breaking wave with a horizontal axis in the lee of the mountain (resulting in the foehn effect and high wind speeds), and the other a periodic vortex with a vertical axis (von Kármán vortex streets) produced beneath a temperature inversion at the margin of the massif. This cooler, denser air effectively prevents the foehn wind from propagating further downslope, restricting the highest temperatures to the lee slope rather than the coast.

Just how strong this temperature inversion can be is demonstrated by comparing air temperatures at each AWS site for days when foehn winds were and were not active. On a fairly typical cold, cloudy day (30 December 2003), an average lapse rate of -10.24 °C km^{-1} for the lower, and -5.85 °C km^{-1} for the upper part of the glacier was recorded, averaging -8.22 °C km^{-1}. In contrast to this, early on 5 February an inversion due to a foehn on the upper slopes was most pronounced with an average lapse rate of -9.17 °C km^{-1} for the lower, and +20.72 °C km^{-1} for the upper glacier (average +4.57 °C km^{-1}). These observations have important implications for any attempt at modeling mass balance, which is discussed in more detail below.

Results and Interpretation

DIGITAL ELEVATION MODEL AND SURFACE AREA CALCULATIONS

We have used the DEM to better define the upper boundary of the glacier, by comparing surface gradients with ice velocity and ice thickness measurements (Fig. 2). There is still considerable uncertainty in defining the upper boundaries where Brown Glacier shares common divides with adjacent glaciers. This is reflected in our error estimates in the area calculations. We calculate the total area of the glacier (January 2004) to be 4.38 ($\pm$0.47) $\times$ 10^6 m^2.

Average surface slopes for the upper glacier are 17.6° (from the glacier headwall beneath Long Ridge to 500 m downglacier), 11.4° for the mid-glacier (500 m to 3500 m), and 16.5° for the lower glacier (3500 m to the terminus at 4800 m). The average surface slope for the glacier is 13.3°.

ICE THICKNESS AND CROSS-SECTIONAL AREA

Most of the GPR results for Brown Glacier revealed ice thicknesses less than 100 m. The maximum recorded thickness was 112 m on the BG35 profile, which also showed that the glacier flows down two small parallel valleys separated by a subglacial ridge (Fig. 2). This effectively reduces the area of the glacier that actively contributes to the glacier terminus position, with the northernmost valley ending in a zone of stagnant ice above the cliff line at the elevation of BG40. The cross-sectional area of the BG35 profile is 6.26 ($\pm$0.22) $\times$ 10^4 m^2.

ICE DYNAMICS AND MASS FLUX

Results of surface ice velocity measurements for both seasons are presented in Table 4. Figure 8 shows the velocity magnitude as a function of distance from the highest point on the glacier through our primary longitudinal survey sites. In season two, greatest velocities were measured during epoch three, with a maximum of 0.168 m d^{-1} at BG45 (0.179 m d^{-1} in 2000) on the lower and steeper part of the glacier. Surface ice velocities decreased by as much as 36% between epochs 3 and 4 (at BG25 from 0.110 to 0.071 m d^{-1}) with an average decrease for all sites of 22% (0.101 to 0.069 m d^{-1}). The greatest velocity of 0.187 m d^{-1} was measured at BG151 during epoch three. The survey marker at this site was lost, and a number of crevasses were revealed later in the season.

The observed velocity changes can be understood in terms of the expected seasonal evolution (e.g. Willis, 1995). Epochs 1 and 2 were both in late winter, before the onset of significant melting, when velocities are expected to be low. The second field season started in early austral spring and proceeded into summer. The onset of significant melting in spring together with an underdeveloped drainage system (e.g. Fountain and Walder, 1998) often leads to the highest velocities of the year. As drainage paths develop, velocities drop again. This is observed during the last epoch. The high winter velocities near the glacier front during all times indicate that, low on the glacier, basal motion is significant all year round. This is also demonstrated by an inverse methods analysis (Truffer, 2004), and it can be explained by the relatively high winter temperatures near sea level that allow for melt and rain events at any time of the year.

Three transverse velocity profiles were measured (at BG25, BG35, and BG40) (Fig. 9) to allow calculation of the total ice flux near the ELA. We initially estimated the ELA to be near BG40,

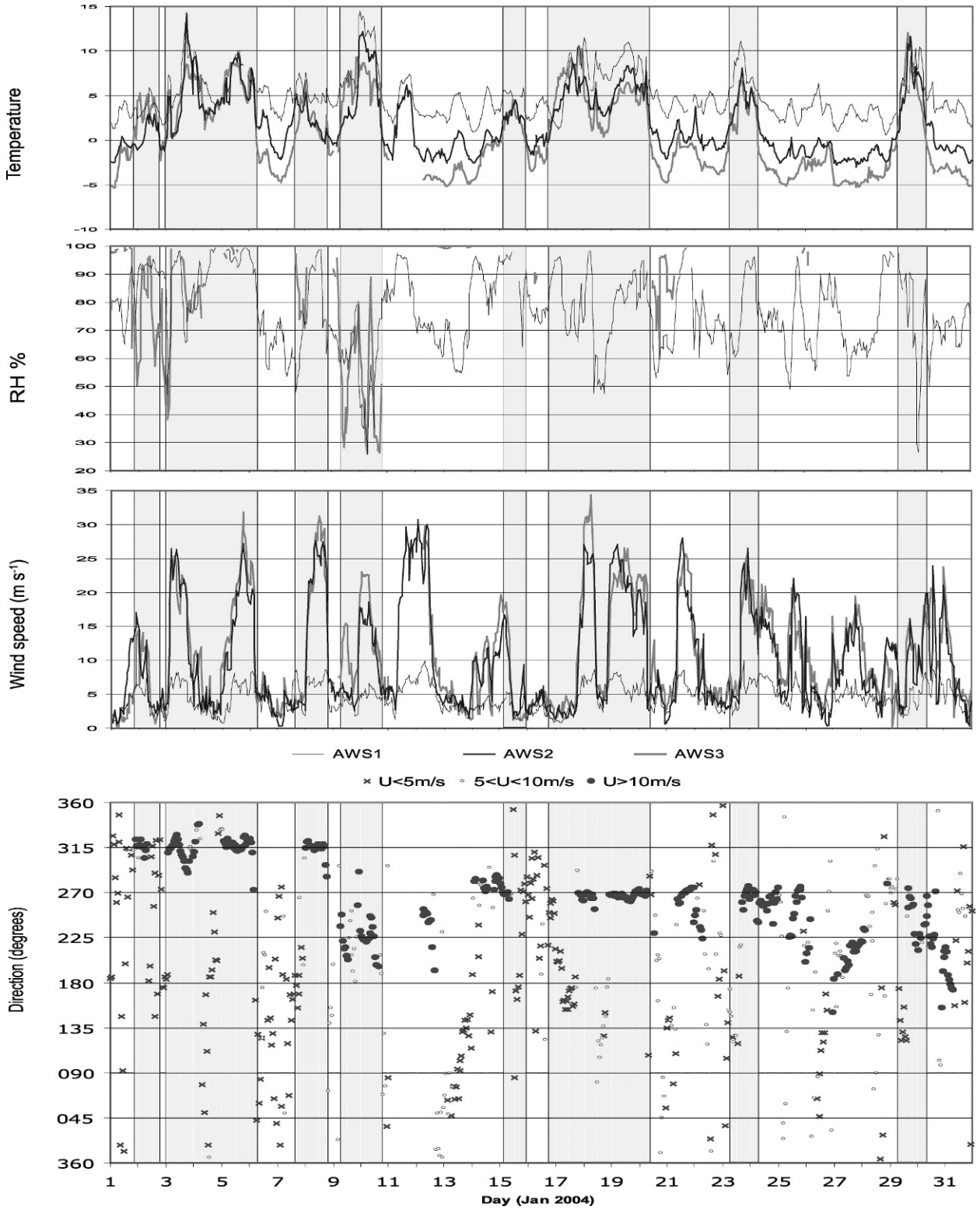

FIGURE 7. Temperature (°C), relative humidity (RH) (%), and wind speed (m s^{-1}) data for January 2004 from the three weather stations adjacent to Brown Glacier. The lower panel plots wind direction at AWS3. Vertical lines and shaded regions mark periods when the air temperature at AWS3 exceeded 0 °C.

based on reports of the end-of-summer snow-line height (Ruddell, 2006). Our field observations suggested it was higher than this. Paterson (1994) quoted an accumulation to total area ratio of 0.7 for a steady-state glacier. Using our new estimates of the glacier area would put the ELA between 525 and 550 m a.s.l. The fact that the glacier is currently in a negative balance puts it even higher. Note that observations of snow-line elevations are notoriously difficult in this climate, as snowfall is able to reach sea level at any time of the year. Eventually we chose the BG35 profile for detailed study because it was less crevassed and easier

TABLE 4

Surface ice velocities (m d^{-1}) at survey sites on Brown Glacier for two epochs during season one (Oct.–Nov. 2000; left) and season two (Dec. 2003–Feb. 2004; right). Epoch 1 (27–28 Oct. to 9–11 Nov. 2000); Epoch 2 (9–11 Nov. 2000 to 21–22 Nov. 2000); Epoch 3 (24–28 Dec. 2003 to 20–26 Jan. 2004); Epoch 4 (20–26 Jan. to 9–12 Feb. 2004).

Season one survey site	Elevation (m a.s.l.)	Surface ice velocity (m d^{-1})		Season two survey site	Elevation (m a.s.l.)	Surface ice velocity (m d^{-1})	
		Epoch 1	Epoch 2			Epoch 3	Epoch 4
BG05-1	1061	0.061	0.053	BG05-2	1027	0.036	0.032
				BG052	1031	0.082	0.068
BG10	958	0.047	0.050	BG10	952	0.045	0.040
				BG101	969	0.087	0.075
BG15-1	865	0.076	0.065	BG15-2	863	0.091	0.085
				BG151	848	0.187	
				BG152	867		0.073
BG20	755	0.080	0.082	BG20	749	0.094	0.065
				BG201	753	0.086	0.058
				BG202	776	0.072	0.053
BG25	678	0.082	0.084	BG25	670	0.110	0.071
BG30	586	0.095	0.094	BG30	579	0.123	0.088
				BG301	577	0.123	0.088
BG35	498	0.125	0.120	BG35	490	0.136	0.097
BG40	414	0.158	0.155	BG40	404	0.156	0.120
BG45	304	0.175	0.179	BG45	293	0.168	0.146
BG50	187	0.155	0.155	BG50	177	0.150	0.136
			Transverse Profiles				
BG351	494		0.025	BG251	673		0.046
BG352	499		0.058	BG252	675		0.059
BG353	496		0.122	BG253	676	0.097	0.069
BG354	494		0.112	BG254	679	0.074	0.058
BG355	492		0.112	BG255	701	0.065	0.052
				BG256	702	0.042	0.027
BG401	414	0.062	0.049	BG257	703		0.027
BG402	415	0.126	0.128	BG258	703		0.037
BG403	414	0.168	0.161				
BG404	418	0.162	0.158				

to work at, as well as being closer to the ELA. The transverse profile (Fig. 9b) shows that the fastest moving ice is somewhat to the southeast of what we picked as the central flowline.

The average velocity (based on our measurements in spring and early mid-summer) along the BG35 profile is 7.5 cm d^{-1} or 27.5 m a^{-1}. With velocities during autumn-winter-spring estimated at 60% of this summer value, average annual velocities across BG35 are more likely to be in the order of 19.2 (±20%) m a^{-1}. Nye (1965) found that the average surface velocity across a transverse profile is within a few percent of the average velocity in a cross section of the glacier. Adopting this assumption, we calculate an ice flux of 1.19 (±0.25) × 10^6 m^3 a^{-1}. This result can be used for comparison with the estimated accumulation and ablation above and below this flux gate.

SURFACE ABLATION: MEASURED AND MODELED

The six-hourly surface position from the SRS results at BG50 and BG35 for January 2004 are presented in Figures 10a and 10b (fine line). At BG50 the SRS recorded a total of 0.16 m accumulation, and −2.18 m of ablation for the month (−0.07 m day^{-1}). The SRS at BG35 only operated for 13 days, recording 0.18 m of accumulation, and −1.52 m of ablation (−0.12 m day^{-1}).

The site survey markers are used to measure specific net balance over a period of time, whereas the SRS data can be resolved into total accumulation and total melt. A comparison between the SRS measurements at BG35 and the co-located survey marker measurement for the first 13 days of January reveals a total ablation underestimate using the survey marker of 0.41 m (0.03 m day^{-1} or 0.93 m for January). This error will be most pronounced at sites that have experienced accumulation and ablation events (i.e. snowfall and snow melt) that were not recorded in the periods between measurements.

Output from the EBM is in total ablation in millimeters of water equivalent (w.e.), and the EBM was first run for the two sites for which SRS data are available and total ablation can be measured. EBM output, using data from AWS1 and 2 (adjusted for elevation) as input (Figs. 10a and 10b, gray lines) is directly compared with results from the SRS at BG50 and BG35. SRS data for BG50 was collected over a melting ice surface and for BG35 over a melting snow surface. Estimates of the surface density at these sites are made that allow direct comparison between the EBM output and SRS data (in reality these "density" estimates also incorporate variations in albedo and z_0 which are held constant for the calculation period). A density of 830 kg m^{-3} at BG50 and 380 kg m^{-3} at BG35 results in the best fit to the observed SRS data, demonstrating that there is good correspondence between the EBM ablation calculations and the measured rates of ablation at both sites (Figs. 10a and 10b).

The EBM was then run twice at each longitudinal site, covering the glacier surface from BG05 to BG50, calculating the total ablation for January: EBM run 1 used an average January lapse rate of −6.2 °C km^{-1} (Allison and Keage, 1986; Fig. 11, line 1) and meteorological variables only from AWS1 as input; and EBM run 2 used hourly lapse rates and meteorological variables derived from the records of all three AWSs adjacent to the glacier

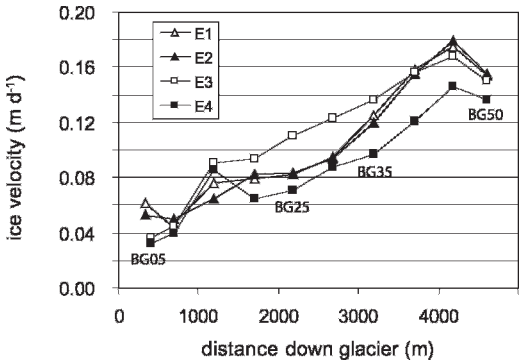

FIGURE 8. Surface ice velocity measurements using DGPS for four epochs (E1–4, defined in Table 4). Longitudinal profile from the upper to lower glacier through the main survey sites.

(Fig. 11, line 2). As expected, there is a significant difference between the two model runs, particularly above 600 m elevation. Modeled ablation using the average monthly lapse rate (run 1) produces a "classic" ablation curve, with totals decreasing with elevation. Using meteorological variables based on values from the three AWSs (run 2) results in modeled ablation totals that show a less pronounced decrease in ablation to ~600 m (BG30), followed by an increase with elevation.

To compare the EBM output with our field measurements again requires an assumption about the surface density at each site. We have used the values that resulted in the best fit of the EBM to the SRS data and applied them to the measured ablation totals for each survey site to convert them to millimeters of w.e. Sites BG05 to BG35 are assigned the value for a snow surface (380 kg m^{-3}), BG45 and BG50 that for ice (830 kg m^{-3}), and BG40 is estimated as being transitional between the two (610 kg m^{-3}). Interpreted this way, the field data lies between the two EBM outputs, closely matching line 2 for the lower three sites, and tending toward line 2 at the upper sites. If we go one step further and add the maximum measured underestimate of monthly ablation at sites BG35 and above (0.93 m snow equivalent), there is a much closer agreement between the EBM output using all the AWS data and our field results (Fig. 11, open diamonds).

This increase in ablation with elevation above ~600 m can be attributed to the effect of foehn winds on the upper slopes of the glacier. This result is a precautionary warning that any attempt at longer term mass-balance modeling must account for, or model the effect of, foehn winds. Relying on coastal AWS data and average free-air lapse rates applied to the whole glacier will result in significant underestimates of total ablation, particularly high on the mountain in the lee of the prevailing winds.

CHANGES TO BROWN GLACIER, 1947–2003

In the 56 years between December 1947 and December 2003, Brown Glacier retreated by 1.17 km at an average rate of 20.9 m a^{-1}. It is reasonable to assume that the retreat rate would not have been steady, and may have been above average while the glacier terminated in water and retreated through the lagoon. The retreat was also much more pronounced on the northwestern side of the glacier (Fig. 4). The total ice covered area has decreased from 6.18 ($\pm$0.47) $\times$ 10^6 m^2 in 1947 to 4.38 ($\pm$0.47) $\times$ 10^6 m^2 in 2004. This corresponds to a loss of ~29% of the original area.

The total ice loss (Fig. 5) was calculated by subtracting the 2004 DEM from the reconstructed 1947 DEM. Using results from the bathymetric survey, Brown Lagoon (with an area of 0.416 km^2 and a maximum depth of $-$56 m) has a volume of 7.8 ($\pm$0.14) $\times$ 10^6 m^3, or about 5% of the total amount of ice lost. The ice volume has decreased by ~1.743 $\times$ 10^8 m^3, (3.06 $\times$ 10^6 m^3 a^{-1}), equating to an average glacier-wide surface lowering of 28.2 m, or 0.50 m a^{-1}. This is a minimum estimate, because ice volume loss was assumed to be zero above 650 m, and no allowance for sedimentation in the lagoon has been made. Our volume loss estimate could therefore underestimate the actual volume change by up to ~25%. This error estimate is based on a 10 m glacier-wide average underestimate in height of the 1947 surface, and a 50% increase in the volume of the lagoon.

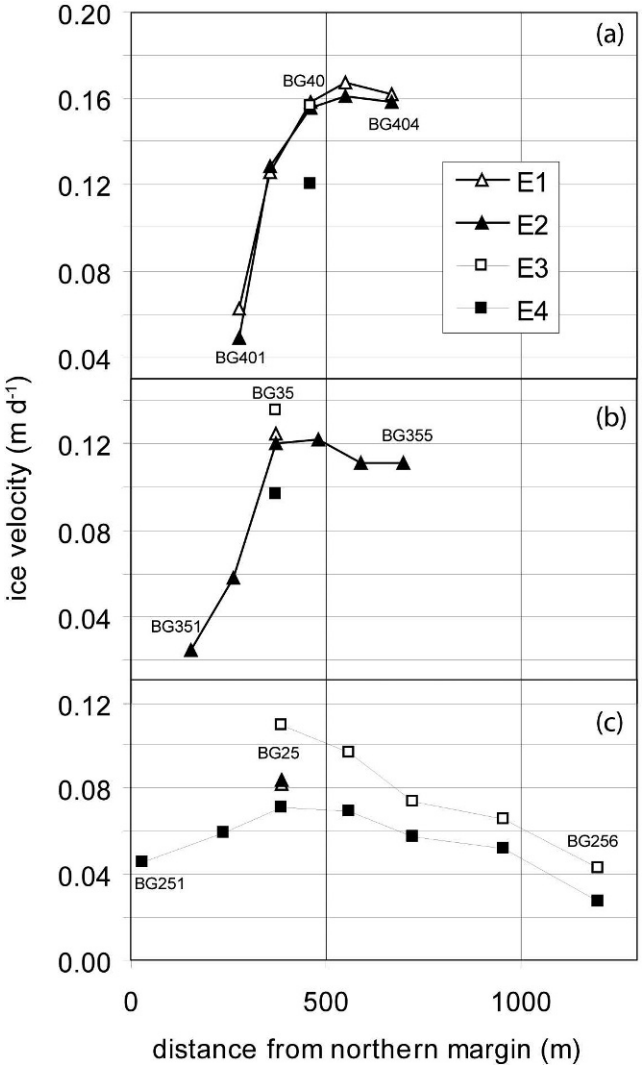

FIGURE 9. Surface ice velocity measurements using DGPS for four epochs (E1–4, defined in Table 4). Transverse profiles across (a) the BG40 survey line (average elevation 415 m), (b) the BG35 survey line (495 m), and (c) the BG25 survey line (689 m).

CHANGES TO BROWN GLACIER, DECEMBER 2000–DECEMBER 2003

A comparison between the terminus surveys undertaken on the 23 November 2000 and the 17 February 2004 shows a marked retreat in the terminus position (Fig. 4). The November 2000 survey was hampered by snow obscuring the ice-rock boundary, with positional errors for the boundary estimated at 20 m. Some snow ramps were still present in December 2003, but the boundary was generally well defined. These problems were not apparent during the February 2004 survey. The average retreat for the east-

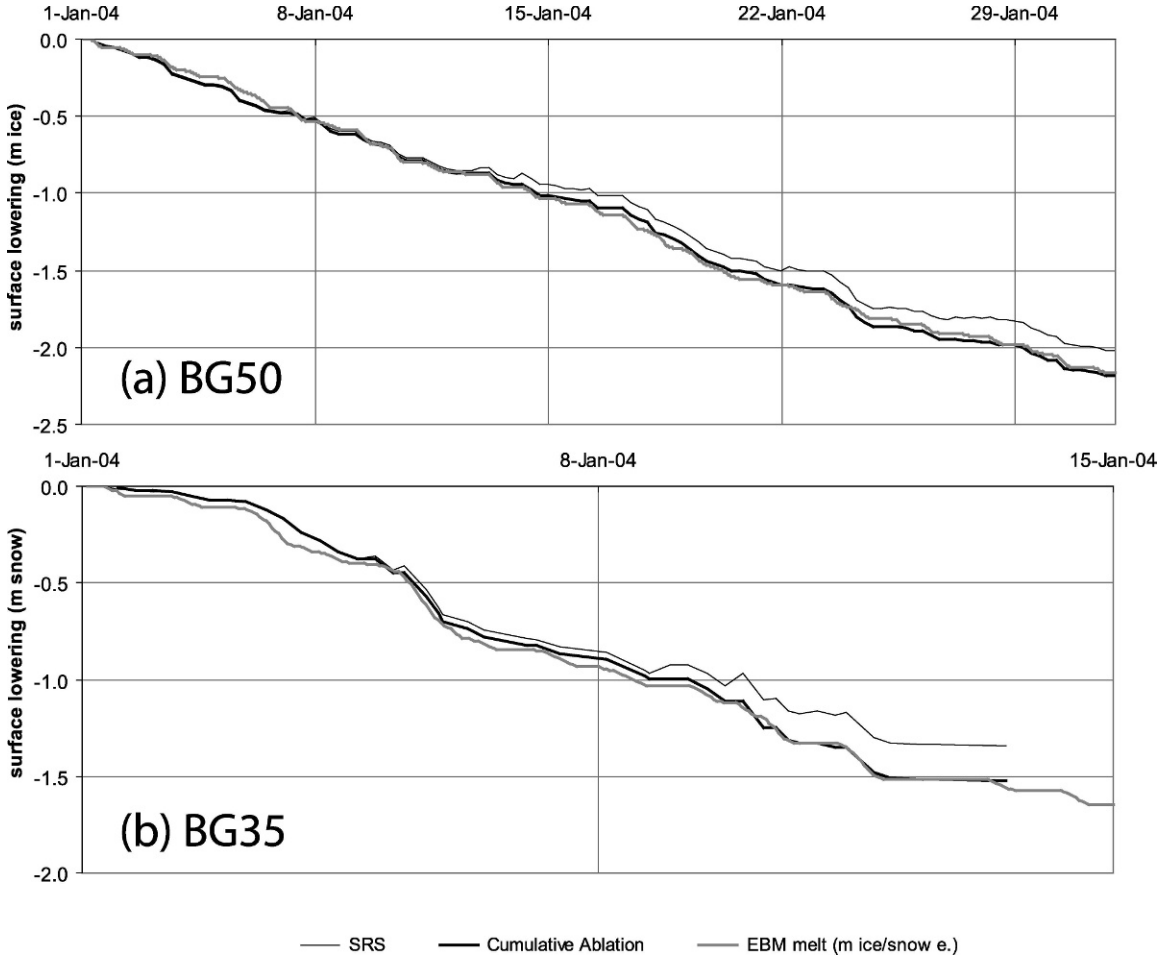

FIGURE 10. SRS data compared with output from the EBM (gray line). Six hourly sonic ranger sensor data for January 2004 (fine line) and the cumulative ablation (black line). (a) Results for BG50, with EBM model output converted to meters of ice equivalent using a density of 830 kg m^{-3}. (b) Results for BG35, with EBM model output converted to meters of snow equivalent using a density of 380 kg m^{-3}. The SRS at BG35 was only operational for the first 13 days of January.

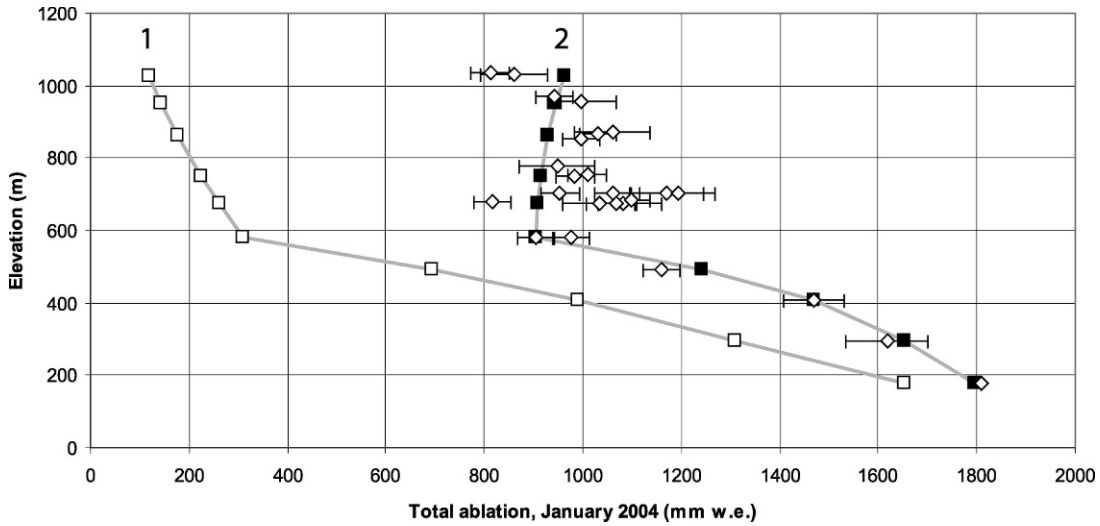

FIGURE 11. Measured and modeled ablation for all survey sites on Brown Glacier, January 2004. Line 1 is the EBM output using meteorological data from AWS1 and a constant lapse rate of $-6.2\ ^{\circ}C\ km^{-1}$. Line 2 is the EBM output using all available meteorological data. Open diamonds plot the total ablation for January measured at each survey site marker, converted to millimeters of water equivalent (mm w.e.) using a density estimate. Sites at 490 m and above are also corrected for underestimating total ablation. Error bars indicate uncertainties associated with interpolating measurements made at the survey markers to the beginning and end of the month. The modeled and observed increase in ablation above 600 m elevation is attributed to the effect of foehn winds. See text for discussion.

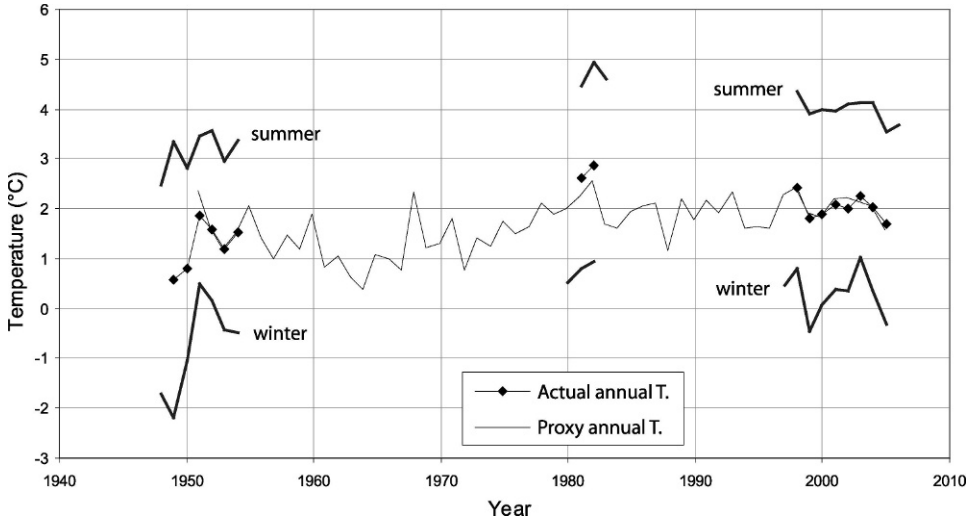

FIGURE 12. Plot of average annual, summer (January–March), and winter (July–September) air temperatures for all years of observation, Atlas Cove. Also shown is a proxy annual temperature for Atlas Cove, based on records from Îles Kerguelen: (Heard Island Proxy annual T) = 1.1662 * (Îles Kerguelen annual T) − 3.6833 ($R^2 = 0.78$). See text for discussion.

facing terminus position, measured in the approximate direction of ice flow (between the November 2000 and the December 2003 surveys), is 63.0 m, equating to 20.3 m a^{-1}. This figure is comparable to the average retreat rate from 1947 to 2003 of 20.9 m a^{-1}, as well as for that between 1980 and 2003 (20.6 m a^{-1}).

A total of 684 crossover points were obtained from the two kinematic surveys undertaken in season one and two. Figure 5 shows the glacier surface to have changed by as much as −11.7 m in the ablation area (average −9.9 m below survey point BG40), and −8.5 m in the accumulation area (average −5.9 m above BG30), equating to an estimated rate of ice loss of $8.0 \pm 1.3 \times 10^6$ m^3 a^{-1}. The error results from an estimated 0.4 m uncertainty in elevation due to correcting the 2004 survey elevations back to late December 2003, and an estimated 1.0 m error from the interpolation between the crossover points. The estimated DGPS surveying errors are in the ±0.15 m range and are therefore negligible.

Discussion

The Heard Island glaciers are undergoing a period of rapid change. Our study of Brown Glacier has revealed significant changes in both the surface area and elevation. In the long-term (1947–2003), the glacier has lost an estimated 29% of its original area with an average ice volume loss of $\sim 3.06 \times 10^6$ m^3 a^{-1}. In the shorter term (2000–2003) our DGPS surveys show the glacier terminus to have retreated on average by 63 m, with a glacier-wide surface lowering equating to continuing ice loss of $8.0 \pm 1.3 \times 10^6$ m^3 a^{-1}. Average surface lowering was 3.3 m a^{-1} below 400 m a.s.l., and nearly 2.0 m a^{-1} above 600 m a.s.l. Whereas it is common that elevation changes are largest at lower elevation (e.g. Arendt et al., 2002), it is noteworthy that even the highest locations on the glacier are thinning significantly.

The most probable cause for the dramatic ice loss of Brown Glacier is an increase in air temperature. Thost and Allison (2006) present evidence that the climate of Heard Island has changed in the last half of the 20th century. Comparison between the 1948–1955 and 1997–2005 epochs show Atlas Cove summer temperatures (January–March) to have increased by 0.8 °C, and winter temperatures (July–August) to have increased by 1.1 °C. The average increase in temperatures for all months between the two epochs was 0.9 °C (Fig. 12; Thost and Allison, 2006; Australian Bureau of Meteorology, unpublished data). There are considerable gaps in the temperature record from Heard Island. Using the record from Îles Kerguelen (MétéoFrance data, Port-aux-Français Station) to reconstruct a proxy temperature record for Heard Island (Jacka and Ruddell, 1999; Thost and Allison, 2006; Fig. 12) suggests that the pattern of warming has not been uniform with time, and there has been considerable variability in the decadal rate of change over this period. The early 1980s were particularly warm (as much as 1.7 °C higher than the 1948–1955 epoch). This variability cautions against over-interpreting a comparison of a 3 year volume change with a 50+ year volume change. Nevertheless, the difference in the rates is striking.

Similar changes are evident over the general region of the Southern Ocean. Jacka and Budd (1998) analyzed temperature data from occupied Southern Ocean sites for the period 1949 to 1996, showing an average warming rate of 0.7 to 1.0 °C $100a^{-1}$. However, for other Southern Ocean stations (Marion Island, Îles Crozet, Îles Kerguelen, and Amsterdam Island), the warming rate was significantly higher at an average of 2.3 °C $100a^{-1}$. The sea-surface temperature record compiled from ship measurements since the 1850s (Bottomley et al., 1990) also shows similar changes for the same period (Ruddell, 2006).

Ruddell and Allison (1998) suggested that a temperature increase of 1.0 °C would be sufficient to explain the observed retreat of Heard Island glaciers over the period of observation (based on results from an unpublished numerical modeling study), and argued that a change in precipitation is an unlikely cause for the glaciers' retreat. Their model required a 31% decrease in precipitation to explain the observed changes in glacier extent, an amount that conflicts with climate models predicting an increase in precipitation in a warmer environment (e.g. Cubasch and Meehl, 2001). Wong et al. (1999) suggested that precipitation minus evaporation over the Indian and Pacific Oceans between 55 °S and 65 °S has increased by $\sim$31 mm a^{-1} over 22 years, which may also be a result of increasing air temperatures. Although there is very high interannual variability in the record of precipitation at Heard Island, the possibility that local precipitation is increasing is given some support by the recent observations of precipitation on the island made by us during January 2004, with rain gauge records from Jacka Valley and Spit Bay returning very high totals in comparison to earlier records from Atlas Cove and Spit Bay. The effect on glacier mass balance of increased precipitation in a warmer climate can be offset to some degree by an increased liquid-solid precipitation ratio.

Big Ben is an active volcano and there is the potential that a higher than normal and a fluctuating geothermal heat flux could affect glacier mass balance and dynamics. Obviously, volcanic eruptions and associated lava flows can have a dramatic effect on glaciers and their bedrock profile. Volcanic activity on the island

has been summarized by Stephenson et al. (2006) who noted that a lava flow from near the summit flowed 8 km down the southwest flank of Big Ben in 1985, nearly reaching the coast, and that the crater within the summit of Big Ben was seen to contain a lava lake in 1986. Other expeditions have noted clouds of steam as well as ash eruptions issuing from the summit (Stephenson et al., 2006; E. Woehler, personal communication, 2004). No activity has been documented for the northeastern quadrant of the island where Brown Glacier is located, in historical times. A simple analysis shows that the melt due to normal geothermal heat amounts to a few millimeters per year (e.g. Paterson, 1994, p. 214). Even an order of magnitude increase of the normal geothermal heat flux would only account for a few centimeters of basal melt. As no measurements of the geothermal heat flux have been made at Heard Island, it is difficult to comment on what the "normal" heat flux is for this area. Using a steady state temperature model, Williams (1998) investigated the effects of a tenfold increase in the geothermal heat flux (from 50 to 500 mW m^{-2}) for two glaciers on Heard Island, calculating an increased contribution in melt rates of between 2 and 5% at the ELA. In contrast to this modest contribution, an air temperature increase of 1 °C resulted in a 38% increase in melt rates at the ELA (Williams, 1998).

If the direct mass balance effect of melting at the base of the glacier due to an elevated heat flux is only minor, what of the contribution of the extra water to the dynamics of the glacier itself? Sturm (1995) observed that a glacier on Mount Wrangell in Alaska did not show pronounced seasonal velocity fluctuations, as is typical of other glaciers in the area. He attributed this to the high volcanic activity of the mountain and proposed that a large volume of subglacial water can be sustained all year-round, a product of the higher than normal geothermal heat flux. Typically the subglacial drainage system undergoes seasonal fluctuations that influence basal motion. It is difficult to compare the early season epochs 1 and 2 directly to later measurements, as they were completed in different years. However the velocity profiles (Figs. 8 and 9) do show a significant decrease from epoch 3 (spring) to epoch 4 (summer), which is consistent with the seasonal development of basal drainage and argues against significant basal melting due to geothermal heat. Also, the outlet stream runs at a much smaller rate in late winter than in spring and summer. We therefore agree with other authors before us (Budd and Stephenson, 1970; Allison and Keage, 1986; Ruddell and Allison, 1998; Williams, 1998; Ruddell, 2006) who considered that the elevated heat flux associated with volcanic activity is not the primary explanation for the widespread glacier recession observed.

Conclusions

Our two field seasons on Heard Island have given us a better understanding of Brown Glacier, but have also revealed many deficiencies that remain in our ability to apply glaciological models without resorting to speculation. In particular, our present understanding of the precipitation regime, even at sea level, is as incomplete as our knowledge of how it changes with elevation on the island, and how snow may be redistributed over the surface. Attempts to study accumulation rates using ion chemistry (Spencer et al., 1985; Donoghue and Allison, 2006) and $\delta^{18}O$ (Truffer et al., 2001; Donoghue and Allison, 2006) on samples collected from the walls of crevasses have been hampered by meltwater percolation and fractionation blurring seasonal signals.

Foehn winds have an effect on the mass balance of Brown Glacier, as well as other glaciers with north-northwest through northeast to southeasterly aspects in the lee of Big Ben. We now know that foehn winds are frequent on the upper slopes of these glaciers, whereas they are rarely observed at the western end of the island. It is not possible to say whether foehn winds have increased in frequency since 1947. They are simply a product of the mountainous nature of the island coupled with the strong winds associated with this latitude, and glaciers in the lee of the mountain have always felt their influence on mass balance. The resultant effect of foehn winds is, however, much more difficult to model. Output from the EBM of Brock and Arnold (2000) coupled with data from three weather stations at different elevations adjacent to Brown Glacier shows that in such a dynamic atmospheric environment, using simple free-air lapse rates to calculate temperature with elevation, even for monthly averages (e.g. Allison and Keage, 1986), will result in errors, underestimating ablation rates at altitude.

Although we lack the year-round data to be more definitive about accumulation rates, surface velocities, and consequently, ice flux estimates, we can make some tentative observations. Using our velocity measurements and our detailed GPR profile at BG35, we estimate the ice flux through this part of the glacier as 1.19 ($\pm$0.25) $\times$ 10^6 m^3 a^{-1}. To balance this flux an average estimated accumulation of 0.35 m a^{-1} (water equivalent) in the area above, and an average ablation of 1.21 m a^{-1} in the area below BG35 is required. Our survey results for the three year period December 2000 to December 2003 show that the overall glacier surface is lowering, indicating the continued retreat of Brown Glacier.

In a simple world of a step change in climate, one would expect volume changes to become smaller in time and approach zero, as the glacier adjusts to a new steady state. Quite the opposite is observed on Brown Glacier. If anything, the rate of ice loss has increased recently by a factor of more than two (from a 1947–2003 average ice loss of 3.1 $\times$ 10^6 m^3 a^{-1}, to a 2000–2003 average of 8.0 $\times$ 10^6 m^3 a^{-1}). While we concede that there may well have been periods of both accelerated and reduced rates of volume change during this period, we conclude that the glacier is reacting to ongoing changes rather than approaching an equilibrium state.

Acknowledgments

We thank Ian Allison for initiating this project and providing valuable input to, and comments on, the many earlier drafts of this paper. The personnel of the two Australian Antarctic Division expeditions to Heard Island provided invaluable assistance in a challenging field environment: in particular Andrew Ruddell, Paul Scott, Don Hudspeth, and Andrew Lock (2000–2001); Shavawn Donoghue, Heather Kirkpatrick, and Robb Clifton (2003–2004). Andrew Fountain and two anonymous reviewers provided constructive criticism on an early version of this paper. Our work is a contribution to Australian Antarctic Science projects 1158 and 2363, and was supported by the Australian Government's Cooperative Research Programme through the Antarctic Climate and Ecosystems CRC at the University of Tasmania. Truffer acknowledges support from NSF grant ANT 335936.

REFERENCES

Allison, I. F., and Keage, P. L., 1986: Recent changes in the glaciers of Heard Island. *Polar Record*, 23(144): 255–271.

Arck, M., and Scherer, D., 2001: A physically based method for correcting temperature data measured by naturally ventilated sensors over snow. *Journal of Glaciology*, 47(159): 665–670.

Arendt, A. A., Echelmeyer, K. A., Harrison, W. D., Lingle, C. S., and Valentine, B., 2002: Rapid wastage of Alaska glaciers and their contribution to rising sea level. *Science*, 297: 382–386.

Barry, R. G., and Chorley, R. J., 1976: *Atmosphere, weather and climate*. 3rd edition. London: Methuen and Co. Ltd, 432 pp.

Bauer, M. H., Mayr, G. J., Vergeiner, I., and Pichler, H., 2000: Strongly nonlinear flow over and around a three-dimensional mountain as a function of the horizontal aspect ratio. *Journal of the Atmospheric Sciences*, 57: 3971–3991.

Beggs, P. J., Selkirk, P. M., and Kingdom, D. L., 2004: Identification of von Karman vortices in the surface winds of Heard Island. *Boundary Layer Meteorology*, 113: 287–297.

Bottomley, M., Folland, C. K., Hsuing, J., Newell, R. E., and Parker, D. E., 1990: *Global Ocean Surface Temperature Atlas*. Norwich: Her Majesty's Stationery Office, 20 + iv pp. and 313 color plates.

Brinkman, W. A. R., 1974: Strong downslope winds at Boulder, Colorado. *Monthly Weather Review*, 102: 596–602.

Brock, B. W., and Arnold, N. S., 2000: A spreadsheet-based (Microsoft Excel) point surface energy balance model for glacier and snow melt studies. *Earth Surface Processes and Landforms*, 25: 649–658.

Budd, G. M., 1964: *The ANARE 1963 expedition to Heard Island*. Melbourne, Commonwealth of Australia: ANARE Reports, Series A (1); narrative, Publication 74, 53 pp.

Budd, G. M., 1970: Heard Island reconnaissance, 1969. *Polar Record*, 15(96): 335.

Budd, G. M., 2000: Changes in Heard Island glaciers, king penguins and fur seals since 1947. *Papers and Proceedings of the Royal Society of Tasmania*, 133(2): 47–60.

Budd, G. M., and Stephenson, P. J., 1970: Recent glacier retreat on Heard Island. *In* Gow, A. E., et al. (eds.), *Proceedings of the International Symposium on Antarctic Glaciological Exploration (ISAGE), September 1968, Hanover, New Hampshire, USA*. International Association of the Science of Hydrology (IASH) Publication 86, 449–458.

Chester, J., 1983: Day of the tempest. *In* Thornton, M. (ed.), *Heard Island Expedition 1983*. Merritt Madden, Sydney: Spirit of Adventure Pty Ltd, 39–41.

Cubasch, U., Meehl, G. A., 39 others, 2001: Projections of future climate change. *In* Houghton, J. T., Ding, Y., Griggs, D. J., Noguer, M., van der Linden, P. J., Dai, X., Maskell, K., and Johnson, C. A. (eds.), *Climate Change 2001: The Scientific Basis. Contribution of Working Group I to the Third Assessment Report of the Intergovernmental Panel on Climate Change*. Cambridge and New York: Cambridge University Press, 881 pp.

Donoghue, S., and Allison, I., 2006: Mass balance measurements of the sub-Antarctic Brown Glacier, Heard Island. *Abstracts of the SCAR Open Science Conference, Hobart, 12–14 July 2006*. 0040/312.

Durran, D. R., 1986: Another look at downslope windstorms. Part I: the development of analogs to supercritical flow in an infinitely deep, continuously stratified fluid. *Journal of the Atmospheric Sciences*, 43: 2527–2543.

Fountain, A. G., and Walder, J. S., 1998: Water flow through temperate glaciers. *Reviews of Geophysics*, 36(3): 299–328.

Green, K., 1993: Heard Island 1992 ANARE report. Kingston, Tasmania: Australian Antarctic Division, unpublished field report.

Jacka, T. H., and Budd, W. F., 1998: Detection of temperature and sea-ice extent changes in the Antarctic and Southern Ocean, 1949–1996. *Annals of Glaciology*, 27: 553–559.

Jacka, T. H., and Ruddell, A., 1999: Construction of a temperature record for Heard Island, and comparison with glacier fluctuations. *In* Meteorology and Oceanography at the Millennium: AMOS '99, Canberra, Australia. Abstracts, p. 32.

Klemp, J. B., and Lilly, D. K., 1975: The dynamics of wave-induced downslope winds. *Journal of the Atmospheric Sciences*, 32: 320–339.

Lilly, D. K., and Zipser, E. J., 1972: The front range windstorm of 11 January 1972—A meteorological narrative. *Weatherwise*, 25: 56–63.

Miller, P. P., and Durran, D. R., 1991: On the sensitivity of downslope windstorms to the asymmetry of the mountain profile. *Journal of the Atmospheric Sciences*, 48: 1457–1473.

Narod, B. B., and Clarke, G. K. C., 1994: Miniature high-power impulse transmitter for radio-echo sounding. *Journal of Glaciology*, 40(134): 190–194.

Nye, J. F., 1965: The flow of a glacier in a channel of rectangular, elliptical or parabolic cross-section. *Journal of Glaciology*, 5: 661–690.

Ólafsson, H., and Bougeault, P., 1996: Nonlinear flow past an elliptic mountain ridge. *Journal of the Atmospheric Sciences*, 53: 2465–2489.

Paterson, W. S. B., 1994: *The Physics of Glaciers*. 3rd edition. Oxford: Butterworth-Heinemann, 480 pp.

Quilty, P. G., and Wheller, G. E., 2000: Heard Island and the McDonald Islands: a window into the Kerguelen Plateau. *Papers and Proceedings of the Royal Society of Tasmania*, 133(2): 1–12.

Ruddell, A. R., 2006: An inventory of present glaciers on Heard Island and their historical variation. *In* Green, K., and Woehler, E. (eds.), *Heard Island: Southern Ocean Sentinel*. Chipping Norton: Surrey Beatty and Sons, 28–51.

Ruddell, A., and Allison, I., 1998: The sensitivity of glaciers at Heard Island to climate change, and their recent response. *In* Selkirk, P. (ed.), *Heard Island Wilderness Reserve: Reports on Natural Science and Cultural Heritage Research*. Kingston, Tasmania: Australian Antarctic Division, ANARE Research Notes 101, p. 32.

Ryan, U., 2004: Heard Island RADARSAT (1997) DEM. Australian Antarctic Data Centre, CAASM metadata (http://aadc-maps.aad.gov.au/aadc/portal/download_file.cfm?file_id=991).

Schär, C., and Durran, D. R., 1997: Vortex formation and vortex shedding in continuously stratified flows past isolated topography. *Journal of the Atmospheric Sciences*, 54: 534–554.

Shaw, P. J. R., 1955: Some effects of topography on weather observations at Heard Island. *Australian Meteorological Magazine*, 10: 34–46.

Spencer, M. J., Mayewski, P. A., and Lyons, W. B., 1985: A preliminary assessment of the potential application of glacio-chemical investigations on Heard Island, south Indian Ocean. *Journal of Glaciology*, 31(109): 233–236.

Stephenson, J., Barling, J., Wheller, G., and Clarke, I., 2006: The geology and volcanic geomorphology of Heard Island. *In* Green, K., and Woehler, E. (eds.), *Heard Island: Southern Ocean Sentinel*. Chipping Norton: Surrey Beatty and Sons, 10–27.

Sturm, M., 1995: Short-period velocity fluctuations of two glaciers on Mt. Wrangell, Alaska. *Physical Geography*, 16(1): 42–58.

Taljaard, J. J., and van Loon, H., 1984: Climate of the Indian Ocean south of 35°S. *In* van Loon, H. (ed.), *Climates of the Oceans*. World Survey of Climatology, 15. Amsterdam: Elsevier, 505–601.

Thost, D. E., and Allison, I., 2006: The climate of Heard Island. *In* Green, K., and Woehler, E. (eds.), *Heard Island: Southern Ocean Sentinel*. Chipping Norton: Surrey Beatty and Sons, 52–68.

Thost, D. E., Truffer, M., and Donoghue, S., 2004: The Heard Island glaciology program 2003–04: studies on the morphology, dynamics, mass balance, and climatic setting of Brown Glacier. Data report. Australian Antarctic Division, unpublished, 28 pp.

Truffer, M., 2004: The basal speed of valley glaciers: an inverse approach. *Journal of Glaciology*, 50(169): 236–242.

Truffer, M., Thost, D., and Ruddell, A., 2001: The Brown Glacier, Heard Island: its morphology, dynamics, mass balance and climatic setting. University of Tasmania, Hobart: Cooperative Research Centre for the Antarctic and Southern Ocean Environment, *Antarctic CRC Research Report*, 24: 27 pp.

Williams, G. D., 1998: The response of Heard Island glaciers to climate change. Unpublished honours thesis. Institute for Antarctic and Southern Ocean Studies, University of Tasmania, Hobart, 113 pp.

Willis, I. C., 1995: Intra-annual variations in glacier motion: a review. *Progress in Physical Geography*, 19(1): 61–106.

Wong, A. P. S., Bindoff, N. L., and Church, J. A., 1999: Large-scale freshening of intermediate waters in the Pacific and Indian oceans. *Nature*, 400: 440–443.

Ms accepted April 2007